Journal of Intelligent & Robotic Systems
https://doi.org/10.1007/s10846-019-01040-y

On the Accuracy of Inertial Parameter Estimation of a Free-Flying Robot While Grasping an Object

Monica Ekal[1] · **Rodrigo Ventura**[1]

Received: 26 June 2018 / Accepted: 15 May 2019

Abstract

When model-based controllers are used for carrying out precise tasks, the estimation of model parameters is key for a better trajectory tracking performance. We consider the scenario of a free-flying space robot with limited actuation that has grasped an object of unknown properties. The inertial parameters - mass, centre of mass and the inertia tensor - of the robot-object system are to be determined. In our previous works, we used a parameter estimation algorithm where truncated Fourier series were used to represent both the reference excitation trajectory and the executed one. That algorithm is the focus of this paper, along with a study of the factors that could contribute to a loss of accuracy in the obtained estimates. Simulation results with the Space CoBot free-flyer robot are used to find the causes of the latter: first, a modified version of the minimum condition number criterion is used to generate feasible excitatory trajectories. The results are compared with those given by the maximum information criterion to check for better excitation. Next, an appropriate number of harmonics has to be found for the Fourier series, which will be used to fit the measured data. This is done autonomously, based on the least squares residual. Finally, the relation between input saturation while executing the excitation trajectory and the errors in the resulting parameter estimates is studied.

Keywords Space robotics · Identification · Mobile manipulation · Non-linear control

The planned Lunar Orbital Platform - Gateway (LOP-G) [1] will be a cis-lunar base for assisting moon, mars and deep missions. The station is expected to be unmanned for long periods of time; this makes the use of free-flyers for maintenance inside the station a possibility. Free-flying robots would also be used for transportation of loads between the cargo ship and the station. These tasks are precise and due to the coupling that exists between the dynamics of the robot manipulator and its base, they demand high-level controllers based on the knowledge of the system model. This is also relevant for free-flying robots like the NASA free-flyers SPHERES [2] and Astrobee [3], which are intended to function in the interior of the International Space Station. Collisions during transportation of payloads whose inertial parameters are not known *a priori* must be strictly prevented. Therefore, accurate knowledge of system parameters is necessary to accomplish such tasks.

1 Introduction

The problem of parameter identification is not new. In the literature, methods based on the Newton-Euler equations of motion have been used to tackle this problem in the case of terrestrial fixed manipulators, [4, 6, 7] and quadrotors [8] among others. This method has been extended in case of space manipulator systems in works such as [9], where the virtual manipulator approach has been used for modelling the system. Another approach is to use the property of conservation of momentum. Ma et al. [10] have used angular momentum conservation to estimate inertial parameters of the spacecraft only, with knowledge of the payload and arm parameters. In works such as [11],

This work was supported by the Fundação para a Ciência e a Tecnologia (FCT) project [UID/EEA/50009/2013]

✉ Monica Ekal
mekal@isr.tecnico.ulisboa.pt

Rodrigo Ventura
rodrigo.ventura@isr.tecnico.ulisboa.pt

[1] Institute for Systems and Robotics, Instituto Superior Técnico, Lisbon, Portugal

Published online: 01 June 2019

excitation is provided only in the joints of the arms to identify complete parameters of a manipulator system in the free-floating mode. However, they have used momentum control devices to maintain non-zero angular momentum for free-floating systems. In [12], Kazuya et al. have used the effect of the gravity gradient torque to complement parameter estimation based on momentum conservation in free-flying mode. Rackl et al. [13] as well as Morutso et al. [14] have compared the performance of existing methods based on the two above-mentioned approaches.

The methods in the above-mentioned works are, in general, looking to estimate a maximum number of parameters of the robot base and the manipulator. For the methods based on angular momentum conservation, the space manipulator robots are considered in free-floating mode. Due to this, external forces and torques can be taken as zero. Additionally, acceleration and joint torques would not be required, which are noisy and difficult to measure, respectively. However, obtaining a linear form with respect to the parameters to be estimated is more straightforward in the eqs.-of-motion approach.

Our proposed method, [15], is inspired from [4] and [7], where parameter identification of ground-based manipulators was carried out using the eqs.-of-motions approach. A Fourier Series fit of the measured data is analytically differentiated to give the velocities and accelerations. Noise-inducing numerical differentiation of the measurements is avoided in this way.

Moreover, in our case, the robot is a free-flyer grasping an unknown object, and the inertial parameters of the complete system remain to be determined. We propose to keep the manipulator fixed at a position, while excitation is provided in the inertial space only. This helps to circumvent the difficulty in measurement of joint torques. Unlike reference [7] which uses a band-limited position-feedback controller, we cannot ensure that the measured data is band-limited. This is one of the points where our proposed method differs from the references mentioned above : we use more harmonics in the filtering and Fourier fitting of the measured data, than the number that the reference trajectory had. We also ensure that the excitation is tracked while accounting for actuation limits. Consequently, input saturation is experienced at times, which might have a detrimental effect on the accuracy of the estimates. For simplicity, this work considers the unmodeled load to be attached directly to the base. Extending the problem to include the manipulator arm would not be an issue, given that no excitation is provided in the joint space.

This paper is an extension of the work originally reported in ICARSC 2018 [16], in which an energy-balance based approach was used to calculate the number of harmonics to be used in the filtering and Fourier Series fit of measured data. The main contributions of this paper are:

1. Least square residual error for finding the number of harmonics
2. Modified condition number criteria for improved excitation and feasibility
3. A deeper analysis of comparison of the two criteria for excitation and the effects of saturation on the accuracy of the estimates

The paper is structured as follows: Dynamics of the robot are presented in Section 2. The estimation problem is presented in Section 3. Section 4 describes the steps for generation of the excitation trajectories using optimization, and the use of non-linear Model Predictive Control for tracking them. Section 5 lays down the steps involved in finding parameter estimates from the measured data. In Section 6, we present results of our simulations to test potential causes of loss of accuracy in the estimates, while Section 8 provides a summary, concluding remarks and plans for future work.

2 Dynamics of a Free-Flying System

For the sake of simplicity, only the dynamics of the robot have been modeled here. The arm is considered to be static throughout the process. We consider that an unmodeled load is attached directly to the robot. This problem can be extended further to include dynamics of the manipulator.

2.1 Rigid-body dynamics

Consider that the vectors of generated force $\mathbf{F}$ and moments $\mathbf{M}$ for the robot are given as

$$\begin{pmatrix} \mathbf{F} \\ \mathbf{M} \end{pmatrix} = \mathbf{A}\boldsymbol{u} \tag{1}$$

where $\mathbf{A}$ is the $6\text{x}M$ actuation matrix, also known as the mixing matrix, composed of the contributions of each actuation input to the net forces and moments, and u is the vector of actuation inputs. In case of a holonomic free-flying robot, $M \geq 6$, A should have rank 6 and $\boldsymbol{u} = [u_1 ... u_M]^T$. The body frame, $\mathcal{B}$, of the robot is situated at its center of mass, P_c. P_s is the changed center of mass of the system after the grasping action has been performed. Vectors $\boldsymbol{p}_c$ and $\boldsymbol{p}_s$, are the position vectors of these two centers of mass, with respect to the inertial frame $\mathcal{I}$. The vector denoting the offset between them, $\boldsymbol{p}_{off}$, is expressed in the body frame, $\mathcal{B}$, as shown in Fig. 1b. The relation between them is, [5, 6]:

$$\boldsymbol{p}_s = \boldsymbol{p}_c + \mathbf{R}\,\boldsymbol{p}_{off} \tag{2}$$

$$\dot{\boldsymbol{p}}_s = \dot{\boldsymbol{p}}_c + \mathbf{R}\left(\boldsymbol{\omega} \times \boldsymbol{p}_{off}\right) \tag{3}$$

(a) The Space CoBot [20]

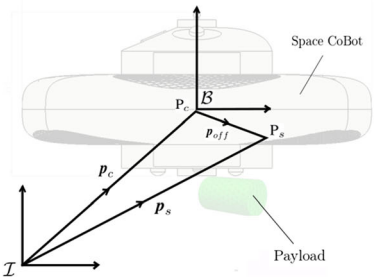

(b) The co-ordinate frames and CoM offset

Fig. 1 An example of a free-flyer robot, the Space CoBot

where $\mathbf{R}$ is the rotation matrix of frame $\mathcal{B}$ with respect to $\mathcal{I}$. $\mathbf{R}$ is in the SO(3) matrix group, i.e, it is a 3×3 real matrix, such that $\mathbf{R}^T\mathbf{R} = \mathrm{I}$ and $det(\mathbf{R}) = 1$ [17].

Newton-Euler equations for the acceleration of the vehicle's center of mass P_c with respect to the inertial frame and the rotation of system in the body frame are derived as [6]:

$$m\left\{\ddot{\boldsymbol{p}}_c + \mathbf{R}\left(\dot{\boldsymbol{\omega}} \times \boldsymbol{p}_{off} + \left(\boldsymbol{\omega} \times \left(\boldsymbol{\omega} \times \boldsymbol{p}_{off}\right)\right)\right)\right\} = \mathbf{RF} \quad (4)$$

$$\mathbf{J}_s\dot{\boldsymbol{\omega}} + \boldsymbol{\omega} \times \mathbf{J}_s\boldsymbol{\omega} + \boldsymbol{p}_{off} \times \mathbf{F} = \mathbf{M} \quad (5)$$

where m stands for mass of the system, $\mathbf{J}$ for its moment of inertia and the operator $\times$ denotes cross product. $\boldsymbol{\omega}$ is the angular velocity of the vehicle expressed in the body frame $\mathcal{B}$.

3 Estimation of Parameters

In this section, we describe the method for estimation of inertial parameters using measured data. As done in [6], the parallel axis theorem can be used to express $\mathbf{J}$ about the origin of body frame P_c instead of the robot-object system's center of mass P_s as:

$$\mathbf{J}_c = \mathbf{J}_s + m\left[(\boldsymbol{p}_{off}^T\boldsymbol{p}_{off})I - (\boldsymbol{p}_{off}\boldsymbol{p}_{off}^T)\right] \quad (6)$$

Substituting (4) in Eq. 5 and using Eq. 6, we obtain:

$$\mathbf{J}_c\dot{\boldsymbol{\omega}} + \boldsymbol{\omega} \times \mathbf{J}_c\boldsymbol{\omega} + m\boldsymbol{p}_{off} \times \mathbf{R}^{-1}\boldsymbol{p}_c = \mathbf{M} \quad (7)$$

Further, $\mathbf{J}_c\boldsymbol{\omega}$ can be written as

$$\mathbf{J}_c\boldsymbol{\omega} = [*\boldsymbol{\omega}]\begin{bmatrix} J_{xx} & J_{xy} & J_{xz} & J_{yy} & J_{yz} & J_{zz} \end{bmatrix}^T \quad (8)$$

where,

$$[*\boldsymbol{\omega}] = \begin{bmatrix} \omega_x & \omega_y & \omega_z & 0 & 0 & 0 \\ 0 & \omega_x & 0 & \omega_y & \omega_z & 0 \\ 0 & 0 & \omega_x & 0 & \omega_y & \omega_z \end{bmatrix} \quad (9)$$

Similarly,

$$\mathbf{J}_c\dot{\boldsymbol{\omega}} = [*\dot{\boldsymbol{\omega}}]\begin{bmatrix} J_{xx} & J_{xy} & J_{xz} & J_{yy} & J_{yz} & J_{zz} \end{bmatrix}^T \quad (10)$$

The Newton-Euler equations thus become linear in terms of the inertial parameters to be estimated. They can be written in a compact form as:

$$\boldsymbol{\gamma}(\mathbf{X}, \dot{\mathbf{X}}, \ddot{\mathbf{X}})\boldsymbol{\pi} = \boldsymbol{\tau} \quad (11)$$

where $\boldsymbol{\gamma}(\mathbf{X}, \dot{\mathbf{X}}, \ddot{\mathbf{X}})$ is the regressor matrix with $\mathbf{X} = [x, y, z, \phi, \theta, \psi]$, and ψ, θ, ϕ being the Z-Y-X Euler Angles used to express orientation relative to frame $\mathcal{I}$,

$$\boldsymbol{\gamma} = \begin{bmatrix} \mathbf{R}^{-1}\ddot{\boldsymbol{p}}_c & \mathbf{S}(\dot{\boldsymbol{\omega}}) + \mathbf{S}(\boldsymbol{\omega})\mathbf{S}(\boldsymbol{\omega}) & \mathbf{0}_{3\times 6} \\ \mathbf{0}_{3\times 1} & -\mathbf{S}(\mathbf{R}^{-1}\ddot{\boldsymbol{p}}_c) & [*\dot{\boldsymbol{\omega}}] + \mathbf{S}(\boldsymbol{\omega})[*\boldsymbol{\omega}] \end{bmatrix} \quad (12)$$

with $\mathbf{S}(\boldsymbol{\omega})$ representing the skew-symmetric matrix,

$$\mathbf{S}(\boldsymbol{\omega}) = \begin{bmatrix} 0 & -\omega_z & \omega_y \\ \omega_z & 0 & -\omega_x \\ -\omega_y & \omega_x & 0 \end{bmatrix} \quad (13)$$

The 10x1 vector of the parameters to be estimated, $\boldsymbol{\pi}$, is

$$\boldsymbol{\pi} = \begin{bmatrix} m & m\mathbf{p}_{off}^T & J_{xx} & J_{xy} & J_{xz} & J_{yy} & J_{yz} & J_{zz} \end{bmatrix}^T \quad (14)$$

and $\boldsymbol{\tau}$ is the vector of the applied forces and moments

$$\boldsymbol{\tau} = \begin{bmatrix} \mathbf{F} \\ \mathbf{M} \end{bmatrix} \quad (15)$$

When N measurements of the states $\mathbf{X}$ (x, y, z and Euler angles, ϕ, θ, ψ) are available, a least square problem can be set up as

$$\mathbf{W}\boldsymbol{\pi} = \mathbf{b} \quad (16)$$

where

$$\mathbf{W} = \begin{bmatrix} \boldsymbol{\gamma}(X(1), \dot{X}(1), \ddot{X}(1)) \\ \vdots \\ \boldsymbol{\gamma}(X(N), \dot{X}(N), \ddot{X}(N)) \end{bmatrix} \quad (17)$$

and

$$\mathbf{b} = \begin{bmatrix} \tau(1) \\ \vdots \\ \tau(N) \end{bmatrix} \quad (18)$$

If the N measurements $\mathbf{X}$, their velocities and accelerations can be assumed to be devoid of noise, then the matrix $\mathbf{W}$ can be said to be noise-free. The data-processing steps in

Section 5 attempt to filter out noise from the measurements, such that this assumption holds. The solution vector $\hat{\boldsymbol{\pi}}$ is then given by the maximum likelihood estimation in Eq. 19. The weights are the reciprocal of $\boldsymbol{\Sigma}$, the $6N \times 6N$ diagonal co-variance matrix of the measured forces and torques from time instances 1 to N.

$$\hat{\boldsymbol{\pi}} = (\mathbf{W}^T \boldsymbol{\Sigma}^{-1} \mathbf{W})^{-1} \mathbf{W}^T \boldsymbol{\Sigma}^{-1} \mathbf{b} \tag{19}$$

In this work, we use the desired forces and torques as the measured ones, and consider the measurements to have the same standard deviation, such that Eq. 19 can be written without the weights, as $\hat{\boldsymbol{\pi}} = (\mathbf{W}^T \mathbf{W})^{-1} \mathbf{W}^T \mathbf{b}$.

The regressor matrix, $\mathbf{W}$, must be full-rank. This means that the result of the parameter identification depends on $\mathbf{W}$, which is a function of $\mathbf{X}, \dot{\mathbf{X}}, \ddot{\mathbf{X}}$. Moreover, estimating velocity and acceleration from real data is non-trivial due to sensor noise. Thus, appropriate excitation and measured data processing is needed to obtain a good estimate.

4 Excitation Trajectory

In this section, we summarize the procedure for calculation and tracking of the excitation trajectory. As in [4], the excitation trajectory for each degree of freedom is a finite Fourier series. The Fourier Series are periodic and their bandwidth can be specified. Both of these properties are beneficial at the time of noise filtering.

4.1 Generation of the excitation trajectory

The time varying references for each of the 6 states, $(x, y, z, \phi, \theta, \psi)$ from $\mathbf{X}$ are a sum of n harmonics of sine and cosine functions as:

$$\begin{aligned} X_i(t) &= a_{io} + \sum_{k=1}^{n} \frac{a_{ik}}{\omega_f k} sin(\omega_f k t) - \frac{b_{ik}}{\omega_f k} cos(\omega_f k t) \\ \dot{X}_i(t) &= \sum_{k=1}^{n} a_{ik} cos(\omega_f k t) + b_{ik} sin(\omega_f k t) \\ \ddot{X}_i(t) &= \sum_{k=1}^{n} -a_{ik} \omega_f k sin(\omega_f k t) + b_{ik} \omega_f k cos(\omega_f k t) \end{aligned} \tag{20}$$

From period of the excitation cycle, T_f, the angular frequency ω_f is found as $\omega_f = 2\pi / T_f$. Selection of the period is influenced by factors such as the acceleration limits of the robot. For example, if the robot's acceleration limits are low, then a longer excitation period would allow it to explore the feasible inertial space adequately. This improves the accuracy of the estimates. It is shown in Section 6.6 that using slower and longer trajectories also increases the effectiveness of the harmonics-filtering method. Further, fast paced trajectories for a slowly-accelerating system could cause input saturation which can lead to inaccurate estimates. This is reported in Section 6.5.

As for the selection of n, having a lot of high frequency harmonics in the reference trajectory will result in trajectories that are excessively squiggly. This will not only pose a problem for noise separation by filtering high frequencies, but could also be difficult for tracking. So, the first few low frequency harmonics are preferred.

The Fourier coefficients, a_{io}, a_{ik}, b_{ik} for $k = 1$ to n, and i from 1 to 6 are denoted by vector $\boldsymbol{\delta}$, which is obtained by optimizing one of the two following criteria.

1. V_1, **Minimizing the condition number** of the $\mathbf{W}$ matrix which has been normalized. With a small condition number, the estimation is less sensitive to noise from the measurements. However, minimizing this criteria led to trajectories with commanded positions (in metres) and attitude (in radians) of the order of 10^{-3} or smaller in magnitude, which were not feasible for tracking. To solve this issue, an additional term was added to the cost function. This maximizes the Root Mean Square (RMS) level of each Fourier series wave or the square root of its power. So the complete objective function used is:

$$V_1 = cond(\boldsymbol{\Sigma}^{-0.5} \mathbf{W}) - \sum_{i=1}^{6} q_i \sqrt{\frac{1}{N} \sum_{\eta=1}^{N} |X_i(\eta)|^2} \tag{21}$$

   Where $\boldsymbol{\Sigma}$ is the diagonal co-variance, and N are the number of elements present in each series X_i, from time 0 to T_f. $\boldsymbol{q}$ is the vector of weights given to each of the six terms.

2. V_2, **Maximizing the log determinant of the Fisher information matrix**

$$V_2 = -log \left[\det(\mathbf{W}^T \Sigma^{-1} \mathbf{W}) \right] \tag{22}$$

   This is a measure of the amount of information the measurements give about the variable to be estimated.

Using discrete values of $X(t)$, $\dot{X}(t)$, $\ddot{X}(t)$ from Eq. 20 at $t = 1$ to N, the optimization problem is formulated as:

$$\begin{aligned} \underset{\boldsymbol{\delta}}{\text{minimize}} \quad & V(\mathbf{X}, \dot{\mathbf{X}}, \ddot{\mathbf{X}}) \\ \text{subject to:} \quad & X(1) = 0, \dot{X}(1) = 0, \ddot{X}(1) = 0 \\ & X(N) = 0, \dot{X}(N) = 0, \ddot{X}(N) = 0 \\ & X_{min} \leq X(t) \leq X_{max} \\ & \dot{X}_{min} \leq \dot{X}(t) \leq \dot{X}_{max} \\ & \ddot{X}_{min} \leq \ddot{X}(t) \leq \ddot{X}_{max} \end{aligned}$$

such that the trajectory starts and ends with the robot at rest. The motion of the robot is constrained so that the generated

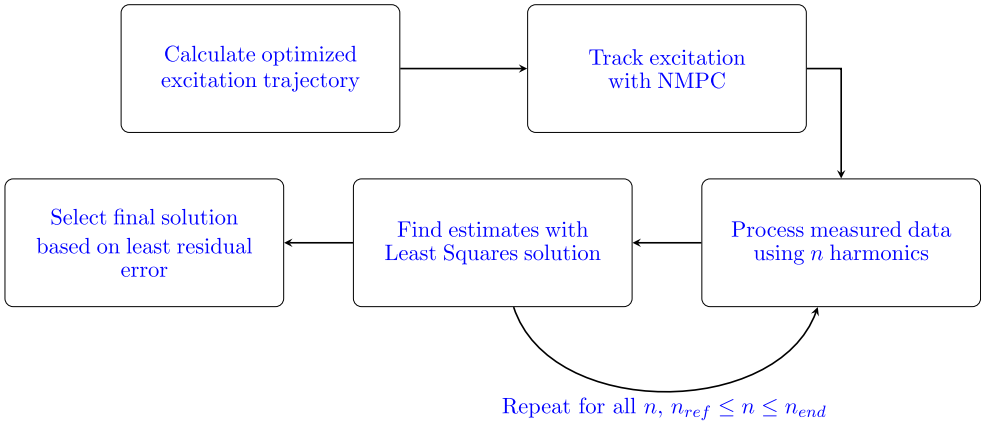

Fig. 2 An overview of the parameter estimation method

trajectory does not have extreme values after optimization of the criteria. Note that this step is independent of the knowledge of the inertial parameters of the robot.

The *Multistart* algorithm with the *fmincon* solver from the Matlab Optimization Toolbox[1] (MathWorks Inc.) was used for finding solutions. The start points were provided manually, because it was found that the local solvers would converge to infeasible solutions if they were run from autonomously generated start points. However, due to the non-convexity of this particular problem structure, different sets of manually provided starting points would result in different local minimum solutions. The relation between the value of the cost function and the accuracy of the estimates is not studied in the scope of this paper. Therefore, instead of finding the lowest of the local minima from a set of start points, we use the solution generated by running the algorithm once from a single start point. These points were chosen as $\boldsymbol{\delta}_0 = rand(1, (2n + 1) \times 6) \times sf$, where the Matlab function *rand* generates a $(2n + 1) \times 6$ row vector of uniformly distributed random numbers between 0 and 1. The number of harmonics of the reference trajectory, as shown in Eq. 20, is n, and sf denotes a scaling factor selected between 0.01 to 0.1.

4.2 Executing the generated trajectory

After calculation of the excitation trajectory, the next step is for the robot to track it. In this work, we use Non-linear Model Predictive Control (NMPC). The controller uses the model of the free-flying robot without the load. The NMPC objective function minimizes the error between the desired and actual states with the least possible actuation over each horizon, t_h. A terminal cost is also added to ensure stability of the closed loop system. The actuation limits of the robot are accounted for as constraints of the minimization problem, as shown below:

$$\begin{aligned}
\underset{X(\cdot),u(\cdot)}{\text{minimize}} \quad & \sum_{T=t}^{t+t_h-1} (\|e(X_{ref}(T), X(T))\|_Q^2 + \|u(T)\|_P^2) \\
& + \|e(X_{ref}(t+t_h), X(t+t_h))\|_{Q_N}^2 \\
\text{subject to:} \quad & \dot{\mathcal{X}} = f(\mathcal{X}(t), u(t)) \\
& u_{min} \leq u(t) \leq u_{max}
\end{aligned}$$

The function $e(X_{ref}(T), X(T))$ denotes the error between the reference and current states. The attitude-tracking controller is based on quaternions to avoid singularities in Euler angle representations. The error function developed by Lee [18] is used for calculating attitude errors. The non-linear model of system dynamics presented in Section 2.1 is represented by $\dot{\mathcal{X}} = f(\mathcal{X}(t), u(t))$, where $\mathcal{X} = [X, \dot{X}]$. Weights of each error in the cost function are denoted Q, Q_N and P. The ACADO toolkit [19] was used to implement this controller.

5 Processing of Measured Data

According to Eqs. 19-18, data gathered at the time of tracking the excitation trajectory is to be used for calculating parameter estimates. The applied forces and torques are needed for $\boldsymbol{\tau}$. It is calculated from the actuation inputs by using Eq. 4. Further, linear and angular velocities as well as accelerations are needed to construct the $\boldsymbol{\gamma}$ matrix. However, estimates of position and orientation obtained from the localization system will be prone to noise. In this case, the velocities and acceleration obtained through numerical differentiation would not be reliable. In this section we present how the periodic and band-limited nature of the excitation trajectory is used to process noisy measured data (Fig. 2).

[1] https://www.mathworks.com/help/optim/index.html

5.1 Noise filtering

An approach similar to that in [4] and [7] has been used here. First, the robot is made to track C cycles (C is taken as 10 in our simulations) of the excitation trajectory. As the excitation trajectory is periodic, the values of positions and attitude are averaged over multiple periods, in order to improve the signal-to-noise ratio of the data. Initial measurement data are usually disturbed by transients. In our case, data from the second cycle onwards is used for calculating average.

Second, the frequencies that were specified for the excitation trajectory are known. Consider an ideal system where only those frequencies would appear in the executed trajectory. In that case, all the other harmonics present in the measured data (all $n > n_{ref}$) would be high frequency noise, and could be discarded. This can be done by: first, finding frequency components of the signal using the Fast Fourier Transform (FFT). Then, the undesired frequencies are filtered out by setting the corresponding phase and amplitude of the higher harmonics to zero, and the rest of the signal is converted back to the time domain.

Note, however, that measurement noise is not the only source of higher frequencies in the executed trajectory. Deviations from the reference caused by nonlinearities in the dynamics of the system will cause high harmonics to show up in the system response. Further, our system has actuation limits, making it vulnerable to saturation. Therefore, a compromise has to be reached between noise rejection and retaining useful data, even if some information is lost in the process.

To tackle this problem, we use a larger number of harmonics, n_{filt}, than the number used in the formulation of the excitation trajectory, for filtering the measured data. That is, the phase and amplitude of all $n > n_{filt}$ are set to zero, and $n_{filt} \geq n_{ref}$. The problem that arises now, is for the algorithm to find the number of harmonics, n, that would best model the executed trajectory while keeping out noise. For this purpose, a method based on the least squares residual is proposed in Section 5.4

5.2 Estimating Fourier Coefficients

Although high frequency noise from the measured data is removed, noise corresponding to the retained frequencies cannot be eliminated. With the selected number of harmonics n, truncated Fourier Series are fitted to the averaged and filtered measured data.

$$\underset{\hat{\delta}}{\text{minimize}} \quad \sum_{\eta=1}^{\mathbf{N}} \|X_{measured}(\eta) - \hat{X}(\eta)\|^2$$

It is known that the least squares fit of a truncated Fourier series is equivalent to finding its Fourier Transform, so the Discrete Fourier Transform can be used instead of a least square problem.

5.3 Finding parameter estimates

Once the Fourier Series co-efficients of the filtered measurements are found, $\hat{\mathbf{X}}_i$, where i = 1,...,6 can be found from the vector of Fourier series co-efficients' estimates, $\hat{\boldsymbol{\delta}}$, by Eq. 20. The values of $\dot{\hat{\mathbf{X}}}_i$ and $\ddot{\hat{\mathbf{X}}}_i$ are found by analytical differentiation of the Fourier Series, so as to avoid differentiating the measurements numerically. Further, the matrix of regressors, $\hat{\mathbf{W}}$ is estimated from Eqs. 12 and 17. Finally, the linear least squares solution, Eq. 19, is used to obtain the parameter estimates, $\hat{\boldsymbol{\pi}}$

5.4 Selecting the number of harmonics

The residual error, $\mathbf{e}$, of the least squares problem from Eq. 16 can be defined as

$$\mathbf{e} = \tilde{\mathbf{b}} - \mathbf{W}\hat{\boldsymbol{\pi}} \tag{23}$$

An ideal number of harmonics should filter out high-frequency noise from the measured data, and provide the least estimation error. It is expected, that the more accurately the inertial parameters are estimated, the closer will be the value of the estimated torques to the measured ones. Thus, the following method is used:

1. The number of harmonics are increased incrementally from n_{ref} (the number of harmonics present in the reference trajectory) to n_{end}, a chosen value, $n_{end} > n_{ref}$. At each value of n, steps given in Sections 5.1, 5.2 and 5.3 are performed, and the value of Eq. 23 is calculated.
2. The value of n at which the norm of the residual error, $||\mathbf{e}||$ is the least, is finally selected as n_{filt}.

It is worth mentioning here, that if the robot faces input saturation while executing the reference trajectory, the errors with respect to the reference will be higher in magnitude. As a result, the effect of high frequency harmonics will be more pronounced in the obtained trajectory. So, intuitively, we can expect the method of filtering and selection of harmonics to yield less accurate estimates when a high amount of saturation is encountered while tracking the reference. This signals a problem, given that the model of the system is not used for planning excitation trajectories, making it difficult to predict saturation before excitation.

6 Simulation Results

In this section, the results of parameter identification of a free-flying space robot in simulation are presented, by considering the Space CoBot free-flyer [20, 21].

6.1 The Space CoBot

The Space CoBot is a free-flying robot, designed with the goal of assisting astronauts in indoor environments, namely inside an orbiting space station. It uses electric propulsion, with 6 motors arranged to provide holonomic motion [20]. It would be used to carry out chores and maintenance on the space station, such as tools and components handling, remote inspection and debris scavenging [21]. This makes it important for the robot to be capable of autonomous grasping and mobile manipulation. It must also be able to navigate safely through the confined spaces of a space station, with or without payload.

6.2 Experimental conditions

In this work, we consider a scenario where the robot has grasped an object and the new inertial parameters of the system are unknown. The mass of the Space CoBot is 6.047 kg. Its inertia tensor is taken to be diagonal, with components $J_{xx} = 0.0453$, $J_{yy} = 0.0417$ and $J_{zz} = 0.0519\ kg - m^2$. Ten excitation trajectories were generated, five each from optimization of criteria V_1 and V_2. These trajectories were obtained by starting the optimization from different points.

The period $T_f = 10$ sec, and $n_{ref} = 3$. The robot was made to track these trajectories for 10 cycles (i.e., 100 seconds). The measurement noise present in the position and attitude measurements is taken to be zero mean Gaussian Noise with a standard deviation of 0.05 for the position and 0.03 for the attitude measurements.

Further, the inertial parameters to be estimated after grasping of payloads were selected from the following normal distributions: A mean (μ) of 7.2 kg for mass, with standard deviation (σ) of 0.5 kg, a μ of 0.0 m for the centre of mass offset, with $\sigma = 0.04\ m$. For the off-diagonal values of the inertia tensor, $\mu = 0.02$ and $\sigma = 0.05\ kg\text{-}m^2$ and for the diagonal values, a mean value of 0.07 $kg\text{-}m^2$, with $\sigma = 0.015$. Ten combinations of these values were used.

Finally, accuracy of estimation of the mass, CoM offset and the inertia tensor elements was compared separately. As a measure of the amount of error between the parameter estimates and the real values, the norm of the errors was used. E.g., the CoM offset error was found as

$$p_{off,error} = \sqrt{\sum_{i=1}^{3}(p_{off,i} - \hat{p}_{off,i})^2} \tag{24}$$

The norm inertia error was found in a similar manner, whereas for mass, simply the absolute error was used. The percentages that these errors formed of the true values of mass/norm of inertia/norm of offset, were used for comparison under different situations.

6.3 Validating the method of harmonics selection

Recall from Section 5.4, that n_{filt} is the number of harmonics that were retained in the measured data at the time of filtering out noise. The value of n_{filt} was selected on the basis of the least residual error, $||\mathbf{e}||$, among all tested harmonics. For the simulations, $n_{ref} = 3$, and $n_{end} = 10$, i.e, the algorithm for harmonics selection tested all harmonics from 3 to 10. Results of the test for one unmodeled load are presented in Fig. 3. The following two lines are plotted as the number of harmonics is increased:

1. Evolution of the error between the parameter estimates and their actual values
2. Change in $||\mathbf{e}||$, which the harmonics selection algorithm uses to find n_{filt}

In real conditions, the actual values of the inertial parameters will not be known *a priori*, and the plots of

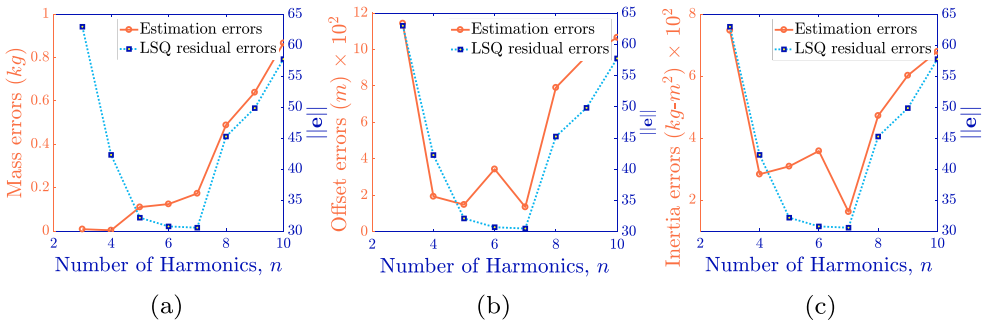

Fig. 3 Evolution of mass, inertia and CoM offset estimation errors, as well as the least square residual error, $||\mathbf{e}||$, as the number of harmonics retained during noise filtering are increased

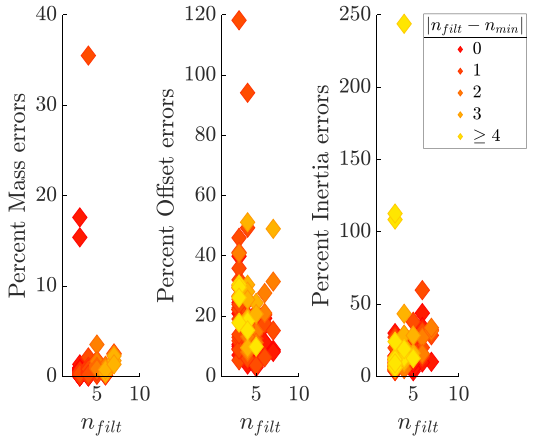

Fig. 4 Parameter estimation results and harmonics needed for 10 loads, each estimated using 10 exciting trajectories

estimation errors are shown simply for comparison and validation. Let the value of n at which the least mass, inertia and CoM offset errors are obtained, be $n_{min,m}$, $n_{min,i}$ and $n_{min,o}$, respectively. For the illustrated case, Fig. 3c and b show that the estimation errors of inertia and CoM offset start to decrease and then increase, with $n_{min,i} = 4$ and $n_{min,o} = 5$. The increase can be attributed to the fact that as more number of harmonics is retained, the efficiency of filtering out high-frequency noise decreases. However, the change in Fig. 3a is different, and the least mass error is obtained at n_{ref}, with $n_{min,i} = 3$.

The figures in Section 3 show that $||\mathbf{e}||$ follows a trend similar to the estimation errors, with $n_{filt} = 7$. It is important to mention here, that while the least error for all parameters might not be obtained with the same n_{min}, only one value of n_{filt} can be chosen. It is up to the harmonics selection algorithm to ensure that the error remains low for all parameters, even when $n_{filt} \neq n_{min}$

In Fig. 4, a compilation of estimation errors obtained with 10 unmodeled loads when they are excited with 10 reference trajectories each, is plotted. The value of n_{filt} is shown on the x-axis, and its absolute difference from $n_{min,m}$, $n_{min,i}$ and $n_{min,o}$ is illustrated using heatmap. It can be seen that the accuracy of estimation has decreased for some loads, and the errors are higher than the rest. The figure also shows that even when $|n_{filt} - n_{min,m/i/off}| \geq 4$, there is no evidence that it results in higher errors for all three parameters, any more than when $n_{filt} = n_{min,m/i/off}$. This validates the harmonics selection algorithm, and it can be ruled out from the potential sources of loss of accuracy. There are alternative explanations for the higher errors. First, it could be that out of the two criteria, one results in poorer excitation that the other. Second, the varying amounts of saturation that the robot's actuation input faced while tracking the excitation trajectories could also lead to less accurate estimates. The next sub-sections will investigate these causes and attempt to find solutions for better estimates.

6.4 Comparison of Criteria for Generating Excitation

As discussed in Section 5.4, the presence of input saturation at the time of tracking the excitation trajectory could result in less accurate estimates. Thus, while comparing the accuracy of estimates using both criteria, we eliminate the bias caused by saturation. This is done by deactivating the limits on actuation. Figure 5 presents the errors between the inertial parameter estimates obtained after optimizing either V_1 or V_2 to generate excitation, and following steps detailed in Sections 4 and 5. Five excitation trajectories from each criteria were used for ten unmodeled loads each. Therefore, 50 results were generated in this manner, and Fig. 5a, b and c were plotted. Figure 5a clearly points to the fact that the mass estimation errors are smaller with criteria V_1.

A paired t-test was conducted to test the alternate hypothesis that the mean of mass estimation errors obtained with criteria V_1 are lesser than those obtained by criteria V_2. The same test was also carried out for CoM offset errors. Statistical significance was obtained in both cases (Mass errors test: t = -8.5162, p-value = $1.568e-11$ and mean of the differences = $-0.0500\ kg$, and CoM offset errors test: t = -1.7166, p-value = 0.0462 and mean of the differences

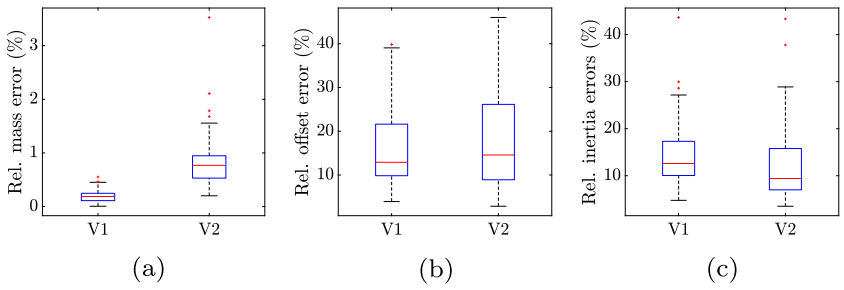

Fig. 5 Relative estimation errors, obtained after excitation was provided with one of the two criteria, V_1 and V_2. Five excitation trajectories were generated per criteria, and each were used for the parameter estimation with 10 cases of normally distributed unmodeled loads. Saturation limits were turned off

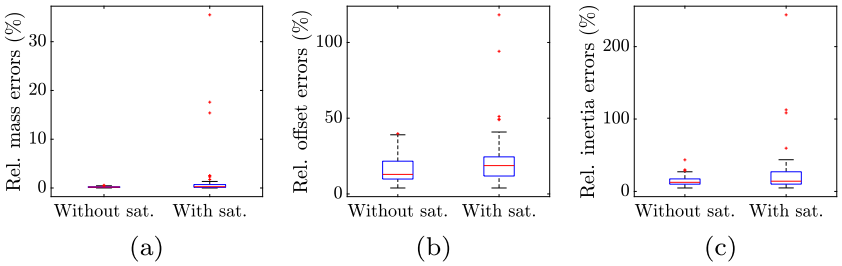

Fig. 6 Relative estimation errors obtained after excitation was provided with criteria V_1, with and without accounting for saturation limits, respectively. Five excitation trajectories were used for the parameter estimation with 10 cases of unmodeled loads with normally distributed paramters

$= -0.0011\ m$). This means that based on the sample data, the average error of mass and center of mass, obtained using V_1 will be lower than that with V_2, at least 95% of the times Even though the median of inertia errors with V_2 seems to be lower than V_1, it results in some outliers with high errors. Based on our results, we select criteria V_1 over V_2. The results reported from this point on only use excitation obtained through V_1.

6.5 The effect of saturation on accuracy of estimates

In a real system, the robot is likely to face saturation while tracking the excitation. Figure 6 illustrates the result of saturation on the accuracy of the estimated parameters. Only those excitation trajectories that were obtained after optimizing V_1 were used. While it is clear that saturation results in more outliers in the estimated data, the magnitude of the outlying errors has also increased. Further investigation showed that these outliers correspond to cases where a lot of saturation was encountered (one or more outputs were at their limits for $>$ 47.75% of the time) per cycle of the excitation trajectory.

Figure 7 gives a better view of what happens as an increasingly saturated excitation is used. The normalized

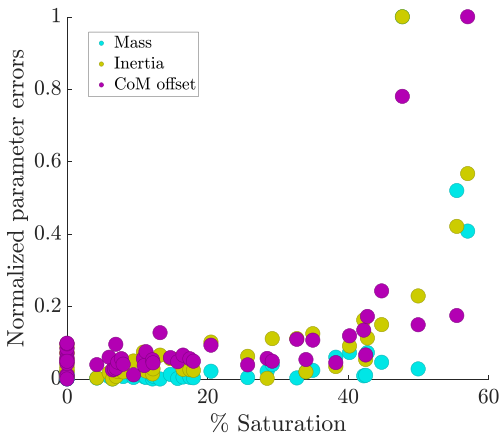

Fig. 7 Change in the accuracy of estimates as input saturation while tracking the excitation increases

estimation errors are plotted in increasing order of input saturation. The vector of errors is normalized separately for each of the three parameters, using the following equation:

$$d_{p,i} = \frac{d_{p,i} - min(\boldsymbol{d}_p)}{max(\boldsymbol{d}_p) - min(\boldsymbol{d}_p)} \tag{25}$$

Here, $\boldsymbol{d}$ stands for the vector of estimation errors. The type of errors (mass, norm of inertia and norm of CoM errors) are represented by p, while i denotes the number of the estimates, from 1 to 50 in this case. Percent saturation is defined as the percentage of time for which at least one of the inputs of the robot was saturated through the course of tracking the excitation trajectory. It is evident that even though it might not happen every time, overall, an increase input saturation results in loss of estimation accuracy.

6.6 Improving the accuracy of the estimates

Section 6.5 showed that the harmonics-based noise rejection method falters at high levels of input saturation. This is due to an increase in the number and magnitude of high frequency harmonics in the composition of the executed trajectory. Still, the estimation errors for CoM offset and inertia parameters in Fig. 6 appear to be high even without saturation. It is to be noted that due to system nonlinearities, the executed trajectory will deviate from the reference one. Fast-paced trajectories would cause more of these deviations. Consequently, each cycle of the obtained trajectory will not be exactly periodic, and spectral leakage effects will occur. Ideally, we would want the obtained trajectory to be as close to the reference as possible.

With that in mind, estimation with slower excitation trajectories was tested on the limited-actuation system. Two trajectories were generated with periods T_f of 60 secs. each. They were used for estimating parameters on the set of 10 simulated loads specified in Section 6.2. Figure 8 shows the resulting relative percent errors, and Fig. 9 plots their absolute values, for a perspective on the magnitude of these errors. Clearly, the estimation errors have now decreased. Thus, even though a longer amount of time is needed for the gathering data, using slower excitation trajectories is

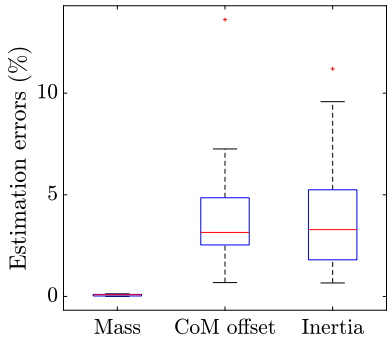

Fig. 8 Relative % estimation errors using excitation with period $T_f = 60$ secs

shown to improve estimation accuracy. Moreover, due to low-acceleration, the system is further away from hitting saturation limits than before. Therefore, determining the value of the excitation period is a trade-off between accuracy of the estimates and the time spent in obtaining them.

7 Discussion

The method proposed in this paper focuses on using a robot excitation trajectory parametrized as a finite Fourier Series, and harmonics based noise rejection. The Least Squares (LS) estimation is used, which offers the advantage of an optimal, closed form solution. In its place, recursive least squares (RLS) can be employed, such that the data are processed after each cycle of the executed trajectory, as opposed to batch processing of data from all cycles. In this way, a priori information about the estimates could also be incorporated. An extension of the RLS approach would be the use of online filters with a propagation model, like the Unscented Kalman filter.

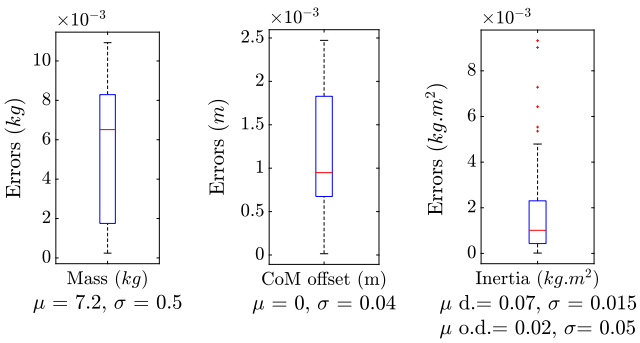

Fig. 9 Absolute estimation errors using $T_f = 60$ secs. excitation. The mean and standard deviation values of the simulated data sets are given for perspective. 'd.' stands for diagonal, and 'o.d' for off-diagonal

8 Conclusion

This paper presented a method of inertial parameter estimation based on Fourier Series excitation and Non-linear Model Predictive Control, and the conditions that can affect accuracy of its estimates. Simulation results of the Space CoBot free-flyer robot were used for this purpose. In the proposed method, the measurement data is processed by filtering out high frequency harmonics and the number of harmonics retained, n_{filt} was shown to have an effect on the results of estimation. The value of n_{filt}, where the least estimation errors are obtained, was found automatically by a method based on the least squares residue. Then, the causes of loss of estimation accuracy were investigated. First, the two criteria for generating excitation, i.e, minimization of the condition number (V_1) and maximizing the information matrix (V_2), were compared in terms of the resulting estimation errors. A modified version of criterion V_1 was used to avoid infeasible trajectories, which maximized the RMS level of each of the 6 Fourier Series, in addition to minimizing the condition number. It was found that optimizing V_1 resulted excitation trajectories that led to better estimates than V_2. Second, the effect of input saturation while tracking the reference trajectory was studied. It was confirmed that high amounts of saturation led to a loss of estimation accuracy, when compared to the less or unsaturated cases. Finally, trajectories with longer periods were found to yield results with a greater estimation accuracy, and proposed as a potential solution for problems caused by input saturation.

Future work will focus on integrating this method in a load transportation scenario. The method will also be tested on a realistic physics engine and in the future, in the real world, on board the International Space Station with NASA's SPHERES or Astrobee free-flyers.

References

1. National Aeronautics and Space Administration, Gateway Memorandum for the Record: A statement from NASA regarding partnerships and development of the Lunar Orbital Platform - Gateway" published May 2 (2018)
2. Miller, D., Saenz-Otero, A., Wertz, J., Chen, A., Berkowski, G., Brodel, C., Carlson, S., Carpenter, D., Chen, S., Cheng, S., Feller, D., Jackson, S., Pitts, B., Perez, F., Szuminski, J., Sell, S.: SPHERES: A testbed for long duration satellite formation flying in micro-gravity conditions. Proceedings of the AAS/AIAA Space Flight Mechanics Meeting (2000)
3. Bualat, M., Barlow, J., Fong, T., Provencher, C., Smith, T., Zuniga, A.: Astrobee: Developing a free-flying robot for the international space station. In: AIAA SPACE 2015 Conference and Exposition (2015)
4. Swevers, J., Ganseman, C., Tukel, D.B., de Schutter, J., Van Brussel, H.: Optimal robot excitation and identification. IEEE Trans. Robot. Autom. **13**(5), 730–740 (1997)

5. Schaub, H., Junkins, J.L.: Analytical mechanics of space systems, American Institute of Aeronautics and Astronautics (2005)
6. Atkeson, C., An, C., Hollerbach, J.: Estimation of inertial parameters of manipulator loads and links. Int. J. Robot. Res. **5**(3), 101–119 (1986)
7. Swevers, J., Verdonck, W., De Schutter, J.: Dynamic Model Identification for Industrial Robots. IEEE Control Syst. **27**(5), 58–71 (2007)
8. Mellinger, D., Lindsey, Q., Shomin, M., Kumar, V.: Design, modeling, estimation and control for aerial grasping and manipulation, 2011 IEEE/RSJ International Conference on Intelligent Robots and Systems, San Francisco, pp. 2668–2673
9. Shin, J.-H., Lee, J.-J.: Dynamic control with adaptive identification for free-flying space robots in joint space. Robotica **12**, 541–551 (1994)
10. Ma, O., Dang, H.: On-Orbit Identification of inertia properties of spacecraft using a robotic arm. J. Guid. Control Dyn. **31**(6), 1761–1771 (2008)
11. Christidi-Loumpasefski, O.O., Nanos, K., Papadopoulos, E.: On parameter estimation of space manipulator systems using the angular momentum conservation, 2017 IEEE International Conference on Robotics and Automation (ICRA), Singapore, pp. 5453–5458
12. Yoshida, K., Abiko, S.: Inertia parameter identification for a Free-Flying space robot, AIAA guidance navigation and control conference and exhibit (2002)
13. Rackl, W., Lampariello, R., Albu-Schäffer, A.: Parameter Identification Methods for Free-Floating Space Robots with direct Torque Sensing. IFAC Proc. Vol. **46**(19), 464–469 (2013)
14. Murotsu, Y., Senda, K., Ozaki, M., Tsujio, S.: Parameter identification of unknown object handled by Free-Flying space robot. J. Guid. Control Dyn. **17**(3), 488–494 (1994)
15. Ekal, M., Ventura, R.: On Inertial Parameter Estimation of a Free-Flying Robot Grasping An Unknown Object, 5th International Conference on Control Decision and Information Technologies (coDIT) (2018)
16. Ekal, M., Ventura, R.: An energy balance based method for parameter identification of a free-flying robot grasping an unknown object, 2018 IEEE International Conference on Autonomous Robot Systems and Competitions (ICARSC), Torres Vedras, pp. 110–116
17. Shuster, M.: A survey of attitude representations. Navigation **8**(9), 439–517 (1993)
18. Lee, T.: Exponential stability of an attitude tracking control system on SO(3) for large-angle rotational maneuvers. Syst. Control Lett. Elsevier **61**(1), 231–237 (2012)
19. Houska, B., Ferreau, H.J., Diehl, M.: ACADO, Toolkit – An Open Source Framework for Automatic Control and Dynamic Optimization. Opt. Control Appl. Methods **32**(3), 298–312 (2011)
20. Roque, P., Ventura, R.: Space CoBot: Modular design of an holonomic aerial robot for indoor microgravity environments. In: 2016 IEEE/RSJ International Conference on Intelligent Robots and Systems (IROS), pp. 4383–4390 (2016)
21. Roque, P., Ventura, R.: A Space CoBot for personal assistance in space stations, IJCAI-2016 Workshop on Autonomous Mobile Service Robots, New York (2016)

Monica Ekal received her M.Sc. in Control Engineering, Robotics and Applied Informatics from Ecole Centrale de Nantes, Nantes, France, in 2016. Her past research has been on control and load transportation using aerial robots. She is currently with the Institute for Systems and Robotics, Instituto Superior Técnico, Lisbon, Portugal, working on estimation and path-planning for free-flying robots in micro-gravity environments.

Rodrigo Ventura (Assistant Professor) received the Licenciatura (1996), M.Sc. (2000), and PhD degree (2008), in ECE from Instituto Superior Técnico (IST), Lisbon, Portugal. He is a (tenured) Assistant Professor at IST, and a member of Institute for Systems and Robotics (ISR). He has several publications in international journals and conferences, on various topics intersecting Robotics and Artificial Intelligence. He is founding member of the Biologically-Inspired Cognitive Architecture society. He participated in several international and national research projects. In particular, he was Principal Investigator of the national project AuReRo (Human-robot interaction with field robots using augmented reality and interactive mapping, 2011-2014), and coordinator of the the IST participation in the EU LdV project USORA (Unified Solution of Remote Access in Practical Vocational Engineering Education, 2013-2015). He is currently Principal Investigator of the national project HARODE (Human-aware service robots for domestic environments). His current research interests include human-robot interaction, human-aware navigation, decision-making under uncertainty, and cognitive robotics, targeting field, service, and space robots. He is the co-author of two national patents on innovative solutions for robotic systems.